MOX–Report No. 34/2013

Automatic computation of the impermeability of woven fabrics through image processing

Tavakoli, A.; Antonietti, P.F.; Verani, M.

MOX, Dipartimento di Matematica "F. Brioschi"
Politecnico di Milano, Via Bonardi 9 - 20133 Milano (Italy)

mox@mate.polimi.it http://mox.polimi.it

Automatic computation of the impermeability of woven fabrics through image processing

Alaleh Tavakoli[a], Paola F. Antonietti[b], and Marco Verani[c]

July 8, 2013

[a] MOX, Dipartimento di Matematica, Politecnico di Milano
Piazza Leonardo da Vinci 32, I-20133 Milano, Italy
E-mail: alaleh.tavakoli@polimi.it

[b] MOX, Dipartimento di Matematica, Politecnico di Milano
Piazza Leonardo da Vinci 32, I-20133 Milano, Italy
E-mail: paola.antonietti@polimi.it

[c] MOX, Dipartimento di Matematica, Politecnico di Milano
Piazza Leonardo da Vinci 32, I-20133 Milano, Italy
E-mail: marco.verani@polimi.it

Abstract

The aim of this paper is to develop a new image-processing based method to compute the impermeability of a given textile, and to propose a mathematical description of the basic knitting procedures together with a mathematical parametrization of the textile structures. The method will be then coupled with a numerical strategy to compute the micro-impermeability of a yarn with the aim of obtaining a multi-scale algorithm that incorporates the effects of the yarn micro-impermeability into the model computing the textile macro-impermeability. Several numerical experiments will assess the validity of our image-processing based approach.

1 Introduction

The permeability is a crucial property of all porous media and in particular it plays a fundamental role in textile manufacturing. Indeed, the availability of reliable mathematical models able to predict the permeability of textiles is of paramount importance to increase the accuracy, efficiency and sustainability of the production process. To accomplish this goal, several different strategies have been proposed in the literature. In the following, we give a brief overview of the state of the art on permeability computation and we identify three different approaches.

The first class of strategies is represented by analytical formulas that have been studied by several authors [4, 3, 7, 6]. A drawback of this approach

is that its validity is limited to simplified textile models. Nevertheless, these formulas are remarkably important to validate the efficiency and reliability of software simulating the intra-yarn permeability.

The second approach is to compute the permeability by directly simulating fluid flows through a given textile model structure. Along this line, Long et al. reduce the three-dimensional fluid problem to a simplified two-dimensional model [17]. This approach is well suited for parametric studies, but, as pointed out in [12], it is not completely clear for which type of textile structures the method is able to predict sufficiently accurate predictions of the permeability. Moreover, accurate predictions can also be obtained by solving a three dimensional (Navier)-Stokes equations or by solving an equivalent lattice Boltzmann model. Simulation tools based on a lattice Boltzmann model use a regular grid and avoid the difficult mesh generation. However, in order to be useful for parametric studies, the calculation of the permeability must be accurate and fast, which is not the case with the available lattice Boltzmann software [2]. On the other hand, the direct solution of the (Navier)-Stokes equations is nowadays standard and it can be performed by employing, e.g., the finite element method (FEM). FEM based simulations deal with non-structured mesh and have the remarkable advantage of handling very complicated geometries. However, the computational effort turns out to be prohibitive since the solvers require the expensive mesh generation of the fluid region between the yarns of the textile.

To circumvent this latter issue, a third class of methods based on homogenization techniques has been recently considered. In particular they employ the Darcy law to build the permeability tensor associated to the textile microstructure and simulate the fluid flow through the homogenized structure employing Stokes, Navier-Stokes or Brinkman equations [15, 13, 14, 16, 12, 5].

In this paper, we present a new method to predict the permeability of textiles, which is representative a new hybrid approach. Indeed, roughly speaking, we combine direct simulation (consistently with the second class of methods discussed above) together with image processing tools. To our knowledge, this mixed approach is new in the literature and we hope it can contribute to the ongoing discussion on the construction of effective methods to predict the permeability of textile structures.

The outline of the paper is as follows. In Section 2 we introduce some notation with a twofold aim: (a) providing the reader with a mathematical description of the basic knitting procedures; (b) introducing a mathematical parametrization of the textile structures. In Section 3 we describe our image-processing based approach to compute the permeability of a given textile which is described in terms of the parametrization introduced in the previous section. In Section 4 we introduce a simple model for the study of yarn impermeability. This model is then employed for introducing in Section 5 the study of an algorithm that incorporates the effects of the yarn

micro-permeability into the model predicting the textile macro-permeability discussed in Section 3.

2 Knitting fundamentals: a mathematical description

Simply stated, knitting is the inter-looping of yarns to form a textile structure. There are two classifications of knits:

> *Weft knitting.* Weft formations have yarns which are knitted across the width of the fabric;
>
> *Warp knitting.* Warp formations have yarns being knitted along the length of the fabric;

see [11] and Figure 1.

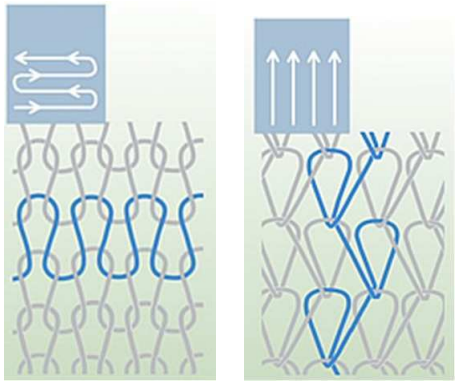

(a) Weft Knit Structure (b) Warp Knit Structure

Figure 1: Knit Structure

2.1 Knitting notation

In this section we review, from a mathematical perspective, some classical notation employed by producers of textile machines to describe knitting procedures. When needed, we will refer to this notation as to the set of *knitting notation*. In the sequel, we will provide the mathematical description of a given textile structure $\mathcal{T}$ by specifying the associated knitting procedure $\mathcal{K}$ used to produce it. As a preliminary step, let us denote by $\mathcal{L}$ a two dimensional lattice of points, each point representing a needle. The mathematical description of the knitting procedure $\mathcal{K}$ is given by specifying the path followed by each yarn between and around the needles of $\mathcal{L}$ (see Figure 2 for a sample of knitting structures)[11]. To accomplish this goal, we number the

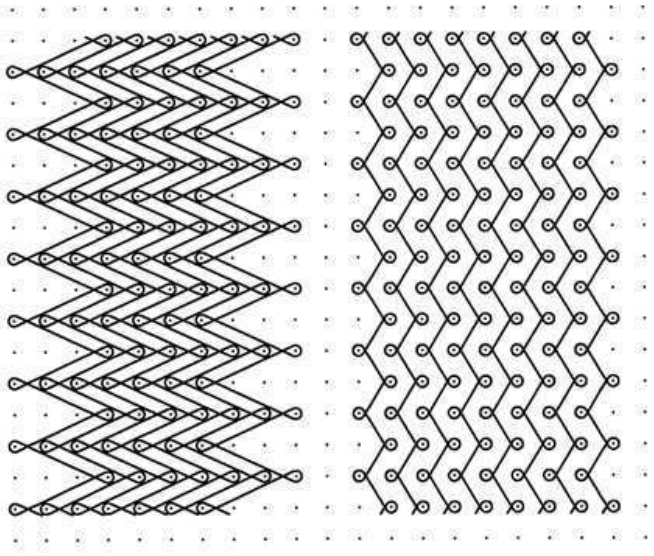

Figure 2: Sample of knitting structures.

spaces between two successive columns of needles as shown in Figure 3, so that each column of needles is uniquely identified by the couple of numbers associated to the the spaces on its left and right, i.e., $(n, n+1)$ or $(n+1, n)$ for $n = 0, 1, 2, \ldots$. In particular, for each of the yarns forming the textile, the

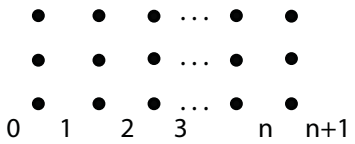

Figure 3: Numbering of the space between needles.

couple $(n, n+1)$ is used to describe the yarn turning clock-wisely around the needle, while the couple $(n+1, n)$ is employed in the case of anti-clockwise rotation. As a last step, we employ the symbol / to describe a shift from one row of needles to the successive one, starting from the bottom of the patch.

Now, we are ready to collect all the above notation and to introduce the concept of *knitting sequence* $\mathcal{S}$. For the ease of the reader, we postpone its formal definition and we start with two simple examples.

Example 2.1 *Knitting sequence* $\mathcal{S}^{(1)} = 1\ 0/1\ 2$. *According to the above discussion, the first couple of numbers* $(1, 0)$ *identifies the first column of needles and specifies that the yarn turns anti-clockwisely around the needle*

located at the first row of the first column. The second couple of numbers $(1, 2)$ *appears after the slash symbol / and thus it specifies that the yarn turns clock-wisely around the needle located at the second row of the second column. The final result is depicted in Figure 4 (left).*

Example 2.2 *Knitting sequence* $\mathcal{S}^{(2)} = 1\ 0/2\ 3$*. The first part of the knitting sequence is the same as before, i.e, the yarn turns anti-clockwisely around the needle located at the first row of the first column. Then, the yarn shift from one row of needles to the successive one and turns clockwisely around the needle located at the second row of the third column. The graphical interpretation of the knitting sequence* $\mathcal{S}^{(2)} = 1\ 0/2\ 3$ *is reported in Figure 4 (right).*

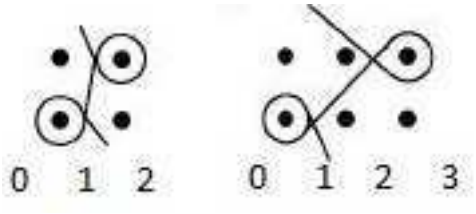

Figure 4: Two examples of knitting sequences: $\mathcal{S}^{(1)} = 1\ 0/1\ 2$ (left) and $\mathcal{S}^{(2)} = 2\ 0/2\ 3$ (right).

We remark that when the knitting sequence changes, for example, from $1\ 0/1\ 2$ to $0\ 1/1\ 2$ the knitting structure changes in a substantial way, passing from what is called *closed knitting* to the *open knitting* (see Figure 5(b)). In this paper we will restrict ourselves to closed knitting structures. Finally,

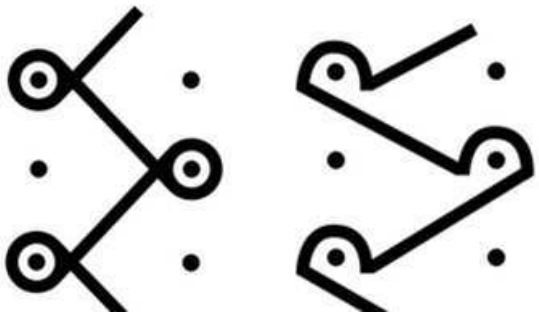

(a) $\mathcal{S} = 1\ 0/1\ 2$ (b) $\mathcal{S} = 0\ 1/1\ 2$

Figure 5: Closed (left) and open (right) knitting structures.

to the sequence $\mathcal{S} = a_1\ b_1/a_2\ b_2$ it is convenient to associate a matrix $\mathbf{Y}_{\mathcal{S}}$

(*knitting matrix*) defined in a natural way as

$$\mathbf{Y}_{\mathcal{S}} = \begin{bmatrix} a_1 & b_1 \\ a_2 & b_2 \end{bmatrix}. \tag{1}$$

In Figure 6 we report the three-dimensional representation of the textile structure obtained by employing the knitting sequence $\mathcal{S} = 1\ 0/2\ 3$ or, equivalently, by the associated knitting matrix $\mathbf{Y}_{\mathcal{S}}$,

$$\mathbf{Y}_{\mathcal{S}} = \begin{bmatrix} 1 & 0 \\ 2 & 3 \end{bmatrix}. \tag{2}$$

cf. (1). We are now ready to state the formal definition of knitting

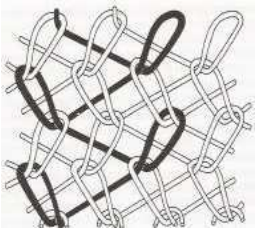

Figure 6: Three-dimensional representation of the textile structure associated to the knitting sequence $\mathcal{S} = 1\ 0/2\ 3$ or equivalenty to the knitting matrix $\mathbf{Y}_{\mathcal{S}}$ given in (2) (Courtesy of [11])

sequence.

Definition 2.1 (Knitting sequence) *A knitting sequence $\mathcal{S}$ is a collection of integer numbers of the type $\mathcal{S} = a_1\ b_1/a_2\ b_2/\ldots/a_n\ b_n$, with associated knitting matrix*

$$\mathbf{Y}_{\mathcal{S}} = \begin{bmatrix} a_1 & b_1 \\ a_2 & b_2 \\ \vdots & \vdots \\ a_n & b_n \end{bmatrix}.$$

We conclude observing that most of the textile structures are obtained by combining two or more knitting sequences $\mathcal{S}^{(i)}$, $i = 1, 2, \ldots$ (see Figure 7 for pictorial representations). This general situation can be easily handled by introducing as many knitting matrices $\mathbf{Y}_{\mathcal{S}^{(i)}}$ as many knitting sequences $\mathcal{S}^{(i)}$ are employed, i.e.

$$\mathbf{Y}_{\mathcal{S}^{(1)}} = \begin{bmatrix} a_1^{(1)} & b_1^{(1)} \\ a_2^{(1)} & b_2^{(1)} \\ \vdots & \vdots \\ a_n^{(1)} & b_n^{(1)} \end{bmatrix}, \qquad \mathbf{Y}_{\mathcal{S}^{(2)}} = \begin{bmatrix} a_1^{(2)} & b_1^{(2)} \\ a_2^{(2)} & b_2^{(2)} \\ \vdots & \vdots \\ a_n^{(2)} & b_n^{(2)} \end{bmatrix}, \qquad \ldots, \qquad \mathbf{Y}_{\mathcal{S}^{(i)}} = \begin{bmatrix} a_1^{(i)} & b_1^{(i)} \\ a_2^{(i)} & b_2^{(i)} \\ \vdots & \vdots \\ a_n^{(i)} & b_n^{(i)} \end{bmatrix},$$

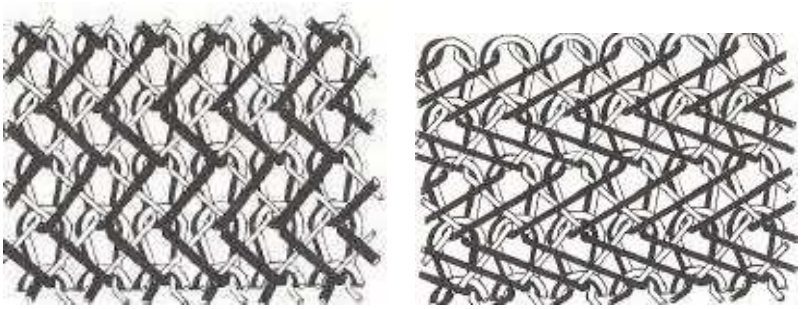

(a) Pictorial representation of the knitting sequence, $\mathcal{S}^{(1)} = 1\ 0/1\ 2$ and $\mathcal{S}^{(2)} = 1\ 2/1\ 0$

(b) Pictorial representation of the knitting sequence, $\mathcal{S}^{(1)} = 1\ 0/2\ 3$ and $\mathcal{S}^{(2)} = 1\ 2/1\ 0$

Figure 7: Textiles structures obtained combining two different knitting sequences (Courtesy of [8]).

2.2 Algorithm `2DFABRIC` : from knitting matrices to textile structures

In this section we introduce and describe the algorithm `2DFABRIC` , that for given knitting matrices builds an (idealized) two-dimensional geometry $\mathcal{G}$ of the corresponding textile. As an example, we consider again the knitting matrix $\mathbf{Y}_{\mathcal{S}}$ associated to to the knitting sequence $\mathcal{S} = 1\ 0/2\ 3$

$$\mathbf{Y}_{\mathcal{S}} = \begin{bmatrix} 1 & 0 \\ 2 & 3 \end{bmatrix}, \tag{3}$$

and in Figure 8 we report the corresponding textile geometry $\mathcal{G}$ generated by our algorithm. The algorithm naturally extends to the case where the

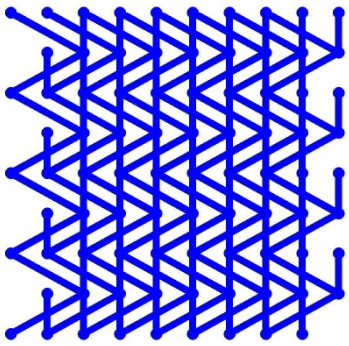

Figure 8: Two-dimensional geometry $\mathcal{G}$ generated by the `2DFABRIC` algorithm corresponding to the knitting matrix $\mathbf{Y}$ defiend in (3).

textile is realized by employing more knitting matrices. For example, let us

consider the following knitting matrices:

$$\mathbf{Y}_{\mathcal{S}^{(1)}} = \begin{bmatrix} 1 & 0 \\ 1 & 2 \end{bmatrix}, \qquad \mathbf{Y}_{\mathcal{S}^{(2)}} = \begin{bmatrix} 1 & 2 \\ 1 & 0 \end{bmatrix}, \quad \mathbf{Y}_{\mathcal{S}^{(3)}} = \begin{bmatrix} 1 & 0 \\ 2 & 3 \end{bmatrix},$$
$$\mathbf{Y}_{\mathcal{S}^{(4)}} = \begin{bmatrix} 1 & 2 \\ 1 & 0 \end{bmatrix}, \qquad \mathbf{Y}_{\mathcal{S}^{(5)}} = \begin{bmatrix} 0 & 1 \\ 2 & 1 \\ 3 & 2 \\ 1 & 2 \end{bmatrix}, \quad \mathbf{Y}_{\mathcal{S}^{(6)}} = \begin{bmatrix} 0 & 1 \\ 2 & 1 \\ 3 & 2 \\ 1 & 2 \end{bmatrix}. \tag{4}$$

In Figure 9 we report the output of our algorithm for different combinations of the above knitting matrices. More precisely, Figure 9(a) and Figure 9(b) are obtained combing the knitting matrices $\mathbf{Y}_{\mathcal{S}^{(1)}}$ with $\mathbf{Y}_{\mathcal{S}^{(2)}}$ and $\mathbf{Y}_{\mathcal{S}^{(3)}}$ with $\mathbf{Y}_{\mathcal{S}^{(4)}}$, respectively, whereas a combination of the knitting matrices $\mathbf{Y}_{\mathcal{S}^{(5)}}$ and $\mathbf{Y}_{\mathcal{S}^{(6)}}$ leads to Figure 9(c). It is worth to notice that the above

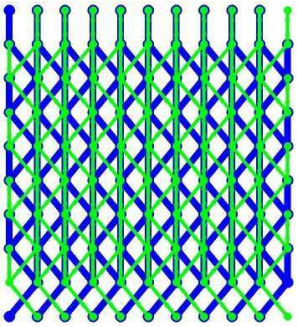

(a) T1: Combination of the knitting matrices $\mathbf{Y}_{\mathcal{S}^{(1)}}$ and $\mathbf{Y}_{\mathcal{S}^{(2)}}$

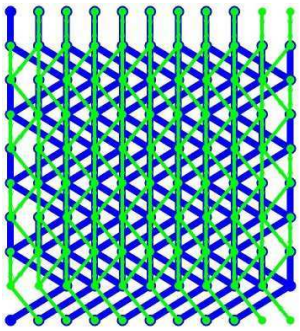

(b) T2: Combination of the knitting matrices $\mathbf{Y}_{\mathcal{S}^{(3)}}$ and $\mathbf{Y}_{\mathcal{S}^{(4)}}$

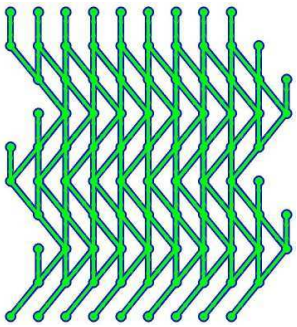

(c) T3: Combination of the knitting matrices $\mathbf{Y}_{\mathcal{S}^{(5)}}$ and $\mathbf{Y}_{\mathcal{S}^{(6)}}$

Figure 9: Two-dimensional geometries generated by the `2DFABRIC` algorithm corresponding to different combinations of the knitting matrices defined in (4).

.

textile structures are prototypal of realistic textiles; in particular, the textiles obtained by employing knitting matrices $\mathbf{Y}_{\mathcal{S}^{(1)}}$-$\mathbf{Y}_{\mathcal{S}^{(2)}}$ and $\mathbf{Y}_{\mathcal{S}^{(3)}}$-$\mathbf{Y}_{\mathcal{S}^{(4)}}$ will be denoted in the following as T1 and T2, respectively; whereas the textile obtained combining the knitting matrices $\mathbf{Y}_{\mathcal{S}^{(5)}}$ and $\mathbf{Y}_{\mathcal{S}^{(6)}}$ will be denoted as T3. We assume, the textiles are possibly realized by made of yarns with different materials and sizes, therefore they have different physical structure. For example, T1, T2 and T3 are assumed to be made of two different kind of yarns: the first is an elastomer, which is an extremely flexible material and the second yarn is a polymeric material, e.g., polyamide.

We conclude this section by detailing the structure of our algorithm `2DFABRIC` which outputs the idealized geometry $\mathcal{G}$ built according to the input of n knitting matrices $\mathbf{Y}_{\mathcal{S}^{(1)}}, \mathbf{Y}_{\mathcal{S}^{(2)}}, \ldots, \mathbf{Y}_{\mathcal{S}^{(n)}}$, together with the thickness values $t^{(1)}, t^{(2)}, \ldots, t^{(n)}$ of the n yarns that compose the textile and the number N of needles employed, cf. Algorithm 1.

Algorithm 1: `2DFABRIC`

Input : $\mathbf{Y}_{\mathcal{S}^{(1)}}, \mathbf{Y}_{\mathcal{S}^{(2)}}, \ldots, \mathbf{Y}_{\mathcal{S}^{(n)}}$: knitting matrices
$t^{(1)}, t^{(2)}, \ldots, t^{(n)}$: thickness of the yarns
N: number N of needles
Output: $\mathcal{G}$

We remark that in the construction of the geometry $\mathcal{G}$ the algorithm neglects the orientation followed by the yarns when they turn around the needles.

3 Textile impermeability

The *impermeability* of a textile is an essential characteristic which is highly influenced by the geometrical structure (or, equivalently, by the associated knitting matrices) of the fabric. A popular methodology for the design of textiles with "optimal" impermeability properties relies on the so-called *trial and error* approach. Accordingly, a large number of impermeability tests (e.g. the Bundersmann test [1]) are performed on fabrics exhibiting different geometrical structures and the data are used to propose new designs to be tested until a satisfactory solution is reached. Clearly, this approach can be very costly.

This section is devoted to propose an alternative automatic strategy based on a numerical algorithm, named `TEXTILE`, that computes the newly introduced impermeability indicator $\mathsf{T}_{\mathsf{imp}}$ quantifying the macroscopic impermeability property of the textile. In particular, the algorithm `TEXTILE` hinges upon the output (idealized) geometry $\mathcal{G}$ of the module `2DFABRIC` , described in the previous section, and computes, via image processing tools applied to $\mathcal{G}$, the area of the region occupied by the yarns. This latter value will be

denoted by $\mathsf{T}_{\mathsf{imp}}$ and represents our impermeability factor. The algorithm `TEXTILE` has the following form:

Algorithm 2: `TEXTILE`

Input : $\mathcal{G}$

1 Image processing of $\mathcal{G}$

Output: $\mathsf{T}_{\mathsf{imp}}$

The image processing step has been implemented by using the software ImageJ [10], while the Java based platform MIJ [9] has been employed to write the interface between ImageJ and the algorithm `2DFABRIC` (written in Matlab). In Figure 10 we report an example of the output of the image processing applied to the idealized textile T1 introduced in the previous section.

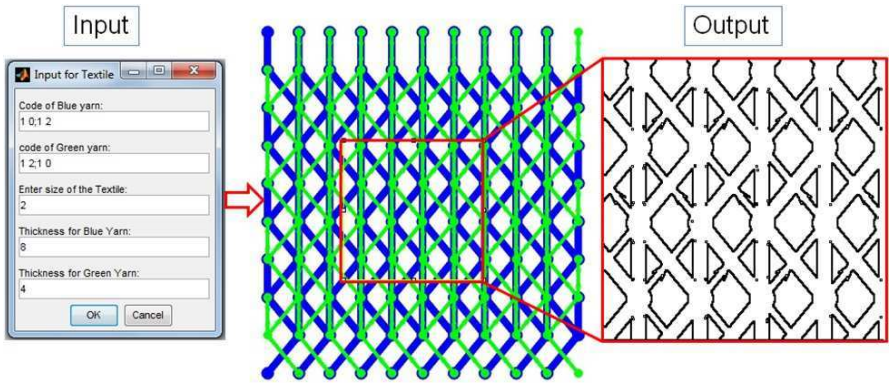

Figure 10: `TEXTILE`: Output of the image processing step for the idealized T1 textile.

Now, we test our algorithm on the textile structures T1, T2 and T3 and we compare the results with the analogous ones obtained by applying `TEXTILE` directly to the pictures of the associated real textiles. It is worth to notice that the pictures have been taken under the same tensile conditions. In Figs. 11-13 we collect the pictures of the real textiles T1, T2 and T3 (middle) and compare the results of the image processing step applied to the output of `2DFABRIC` (left) with the results obtained applying our algorithm directly to the real textiles pictures (right).

Finally, in Table 1 we show the associated computed impermeability factors $\mathsf{T}_{\mathsf{imp}}$. The numerical results obtained working on the idealized structures are in good agreement with the ones obtained with the image processing approach. Indeed, both methodologies are able to detected the most impermeable textile (T3) and the less impermeable one (T1).

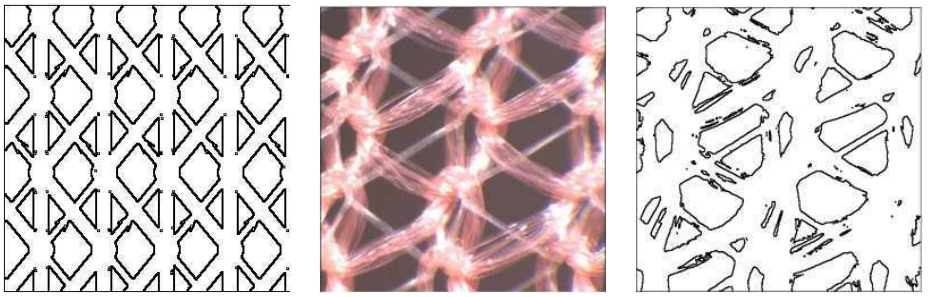

(a) Image processing from `2DFABRIC` (b) Textile T1 (c) Image processing from Textile T1

Figure 11: T1: Output of the image processing step for the idealized (left) and realistic (right) textile.

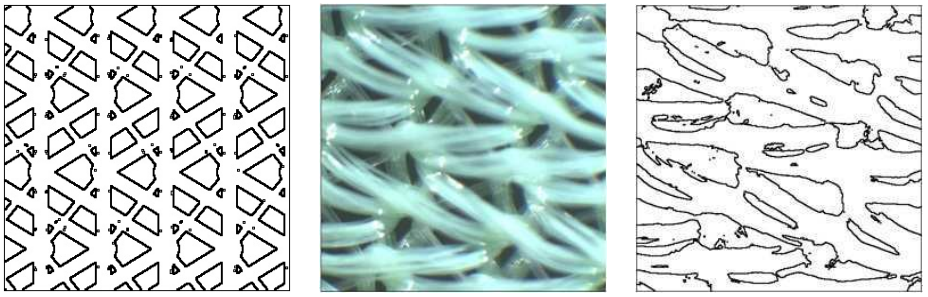

(a) Image processing from `2DFABRIC` (b) Textile T2 (c) Image processing from Textile T2

Figure 12: T2: Output of the image processing step for the idealized (left) and realistic (right) textile.

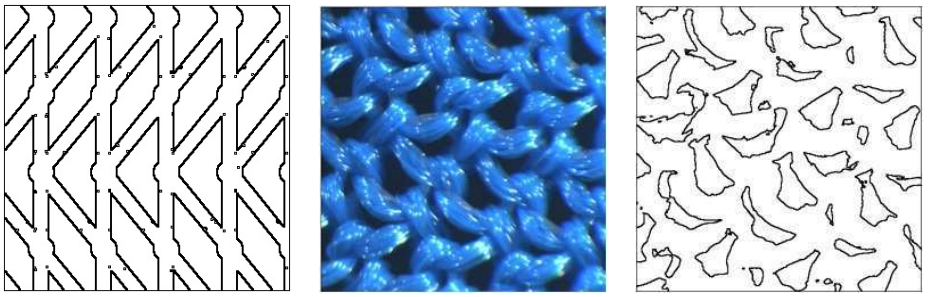

(a) Image processing from `2DFABRIC` (b) Textile T3 (c) Image processing from Textile T3

Figure 13: T3: Output of the image processing step for the idealized (left) and realistic (right) textile.

	T3	T1	T2
$\mathsf{T}_{\mathsf{imp}}$ (From Picture)	229362	226339	225312
$\mathsf{T}_{\mathsf{imp}}$ (From `2DFABRIC`)	78362	74839	74402

Table 1: Impermeability factors $\mathsf{T}_{\mathsf{imp}}$: idealized and realistic textiles.

4 Yarn impermeability

In the previous section we studied the textile impermeability of fabrics under the simplifying assumption that the intra-yarn water flow can be neglected, i.e. the yarns are supposed to be treated as impermeable or, equivalently, to be made of a single fiber. In real industrial applications this is (almost) never the case and each yarn is made of several fibers (see Figure 14 for examples).

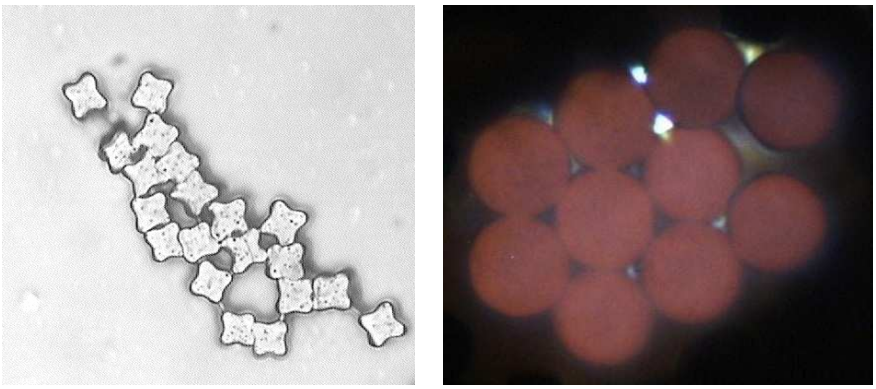

(a) (b)

Figure 14: Fiber geometries (cross sections): (b) quadrilobes; (a) circular (courtesy of Carvico S.p.A).

In this section we fill this gap and we address the impermeability of a single yarn by proposing a numerical strategy able to compute a new yarn impermeability factor, $\mathsf{Y}_{\mathsf{imp}}$, that takes into account also the geometries of the single fibers.

In particular, let $Q = (0,1)^2$ be the unitary square and F_i, $i = 1, \ldots, N$, be the open set describing the cross section of the i-th fiber. Then we define the computational domain as $\Omega := Q \backslash \cup_{i=1}^{N} \bar{F}_i$ (see Figure 15 for an example).

The yarn impermeability factor $\mathsf{Y}_{\mathsf{imp}}$ will be computed, under the assumption that each single fiber is impermeable, by employing the Algorithm 3. More precisely, starting from a given configuration and an initial column of water that is modeled by the quantity $|\mathrm{Area}(\Omega) - \bar{A}|$ (in cf. Algorithm 3), our impermeability factor $\mathsf{Y}_{\mathsf{imp}}$ measures the (discrete) time necessary to the water to pass through the fibers and to exit from Γ_{out}.

Algorithm 3: Computation of $\mathsf{Y}_{\mathsf{imp}}$

Input : Initial domain Ω, relaxation parameter τ

Set $\Omega_0 := \Omega$, $0 < \bar{A} < \text{Area}(\Omega_0)$, $k = 0$

while $|Area(\Omega_k) - \bar{A}| \geq \epsilon)$ **do**

Find (u_k, p_k) such that

$$\begin{cases} -\nu\Delta u_k + \nabla p_k = f & \text{in } \Omega_k \\ \nabla \cdot u_k = 0 & \text{in } \Omega_k \\ u_k = 0 & \text{on } \cup_{i=1}^{M} \partial F_i \cup \Gamma_\ell \\ \dfrac{\partial u_k}{\partial n} - p_k n = 0 & \text{on } \Gamma_{in} \cup \Gamma_{out} \end{cases} \tag{5}$$

Compute

$$y_k := \tau \int_{\Gamma_{out}} \frac{\partial u_k}{\partial n} \mathrm{ds}$$

Update $\Omega_k := (0,1) \times (0, 1 - y_k)$

Update $k = k + 1$

end

Output: $\mathsf{Y}_{\mathsf{imp}} := k\tau$

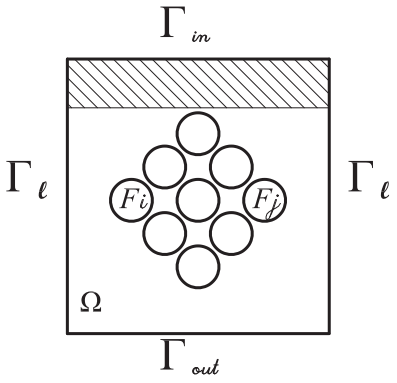

Figure 15: Computational domain Ω for the simulation of the numerical yarn impermeability factor $\mathsf{Y}_{\mathsf{imp}}$. The fiber cross sections $F_1, \ldots, F_9$ are circles. The shadowed region, with area $\bar{A}$, represents the initial column of water.

To approximate problem (5), we employed the stable pair of finite elements $\mathbb{P}^2 - \mathbb{P}^1$ for the velocity and pressure, respectively, and performed

several numerical tests to assess the validity of our approach. We first fixed the value the total area occupied by the fibers and we computed $\mathsf{Y}_{\mathsf{imp}}$ for different choices of the cross section geometries of the fibers. In Figure 16 we show the geometries that have been considered, while the corresponding values of $\mathsf{Y}_{\mathsf{imp}}$ are reported in Table 2. From the results shown in Table 2, it seems that the impermeability increases as the geometrical complexity of the yarn increases. We perform the numerical tests with a tolerance $\epsilon = 10^{-4}$.

In the second set of numerical tests, we fixed the total value of the area

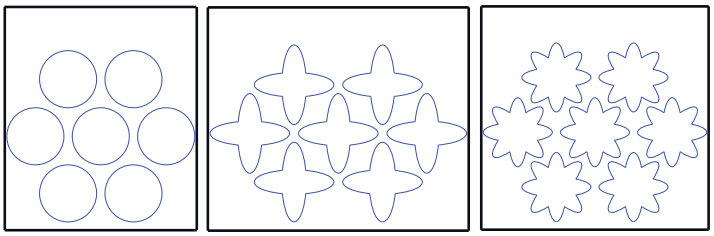

Figure 16: Fibers with different cross-sectional geometriy (Circle, 4-Lobe and 8-Lobe)

	Circle	4-Lobe	8-Lobe
$\mathsf{Y}_{\mathsf{imp}}$	420	445	605

Table 2: Yarn impermeability factor $\mathsf{Y}_{\mathsf{imp}}$ varying the cross section geometry of the fibers.

occupied by the fibers (circular cross section) and we studied the behavior of $\mathsf{Y}_{\mathsf{imp}}$ as the computed of *circular* fibers increases (see Figure 17 for the geometrical configurations). We report the results in Table 3. From our

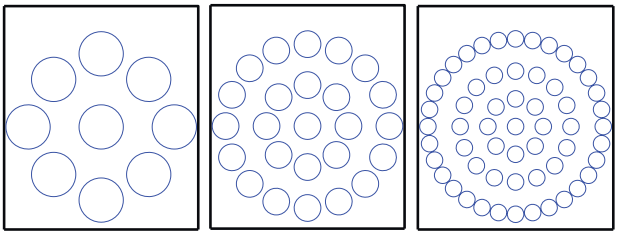

Figure 17: Multi-fiber yarns. From left to right the single yarn is assumed to be made of 9, 25 and 57 circular fibers.

results it can be inferred that the impermeability of a yarn can be increased augmenting the number of fibers.

Finally, with the aim of assessing the *geometrical robustness* of our algorithm we test the sensitivity of the impermeability factor $\mathsf{Y}_{\mathsf{imp}}$ with respect

	9 Fibers	25 Fibers	57 Fibers
$\mathsf{Y}_{\mathsf{imp}}$	80	130	1500

Table 3: Computed yarn impermeability factors $\mathsf{Y}_{\mathsf{imp}}$ as a function of the numbers of circular fibers.

to small variations of the geometrical configuration of the fibers. In particular, the effects of the translation (on the left or on the right) of a single fiber are reported in Figure 18. The results clearly show that our algorithm is able to take into account small geometrical variations of the fiber position.

Remark 4.1 *We note that the yarn impermeability factor* $\mathsf{Y}_{\mathsf{imp}}$ *is computed under some simplifying modeling hypotheses: we employ an idealized geometrical configuration and restrict ourselves to the steady state of the filtration process. Clearly, the model can be enriched by including randomness effects on the geometrical configuration and considering a time dependent framework. This will be addressed in future works. However, as it will be clear in the next section, Algorithm 3 is instrumental to perform the coupling between the micro and the macro impermeability beaviour of a textile. At this level, it can be considered as a black-box procedure providing micro-impermeability and it can be replaced by more sophisticated algorithms (see e.g. [5]).*

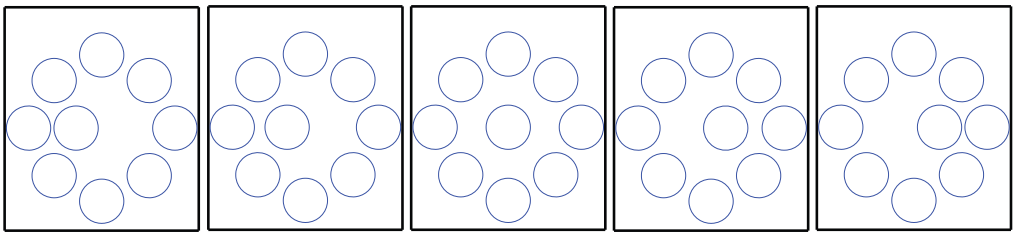

Figure 18: Sensitivity of $\mathsf{Y}_{\mathsf{imp}}$ with respect to fiber position. From left to right $\mathsf{Y}_{\mathsf{imp}}$ =90, 80, 80, 80, 90.

5 Multiscale textile impermeability

We now move a step forward, and incorporate the effects of yarn micro-impermeability into the textile macro-impermeability. This will be achieved by properly choosing the thickness parameters appearing as input variables in the module `2DFABRIC` . In particular, according to the notation introduced in the previous section, we denote by $\mathsf{Y}_{\mathsf{imp}}{}^{(i)}$ the impermeability factor of a multi-fiber yarn made of i circular fibers. Accordingly, $\mathsf{Y}_{\mathsf{imp}} := \mathsf{Y}_{\mathsf{imp}}{}^{(0)}$ denotes the impermeability factor of a single-fiber yarn. In Figure 19 we

report some examples of multi-fiber yarns with circular cross-section. Table 4 shows the corresponding impermeability values computed using the algorithm described in Section 4.

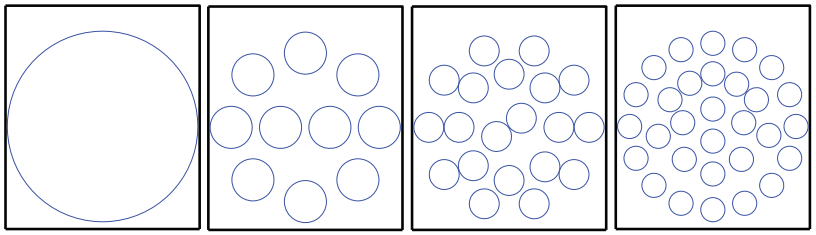

Figure 19: Geometrical configurations: multi-fiber yarns made of $i = 1, 10, 20, 30$ circular fibers.

	1 Fiber	10 Fibers	20 Fibers	30 Fibers
$\mathsf{Y}_{\mathsf{imp}}{}^{(i)}$	16000	120	160	240

Table 4: Yarn impermeability values for multi fiber yarns made by $i = 1, 10, 20, 30$ circular fibers (see Figure 19).

We compute the thickness $t^{(i)}$ of the multi-fiber yarn made of i fibers as:

$$t^{(i)} = \vartheta \frac{\mathsf{Y}_{\mathsf{imp}}{}^{(i)}}{\mathsf{Y}_{\mathsf{imp}}} t_{\text{ref}} \ , \tag{6}$$

where t_{ref} is the reference thickness associated to the single-fiber yarn and ϑ is a proper scaling factor.

We now test our approach with the multi-fiber version of the textiles T1, T2 and T3. In particular, we assume that each variant is realized knitting a single-fiber yarn (with associated thickness value $t = 4$) together with a multi-fiber yarn made of 10, 20 and 30 fibers, respectively. In Table 5 we report the impermeability results together with the thickness values t^i of the multi-fiber yarns that are obtained using a reference thickness value $t_{\text{ref}} = 8$ and scaling factor $\vartheta = 60$. As expected, the impermeability of the textiles increases when multi-fiber yarns (with increasing number of fibers) are employed. In particular, we note that the impermeability of the textile composed by 20 fibers is 11% larger than the one of the T1 textile made up by 10 fibers, while the impermeability of the textile composed by 30 fibers is 26% more than the one of the textile made up by 10 fibers. This in agreement with experimental tests conducted employing the so called Bundesmann test [1].

Fibers i	t^i	T3 $\mathsf{T}_{\mathsf{imp}}$	T1 $\mathsf{T}_{\mathsf{imp}}$	T2 $\mathsf{T}_{\mathsf{imp}}$
10	3.6	75750	69482	67809
20	4.8	76915	71665	70172
30	7.2	78174	74270	73894

Table 5: Impermeability of multi-fiber versions of T1, T2 and T3, $\vartheta = 60$. The textiles are ordered in terms of $\mathsf{T}_{\mathsf{imp}}$ in a decreasing way. The ordering is maintained regardless of the number of fibers.

6 Conclusions

In this paper we proposed a mathematical description of the basic knitting procedures together with a mathematical parametrization of the textile structures. This was instrumental to introduce the main result of this work, i.e., a new image-processing based method to compute the impermeability of a given textile. The proposed methodology has been coupled with a numerical strategy to predict the micro-impermeability of a yarn with the aim of obtaining a multiscale algorithm that incorporates the effects of the yarn micro-impermeability into the model computing the textile macro-impermeability. Several numerical experiments has assessed the validity of the proposed approach.

Acknowledgements

The Authors acknowledge the partial support of the Project "Dote Ricerca Applicata" funded by Regione Lombardia.

References

[1] From the web sites: http://www.daieikagakuseiki.co.jp/en/.

[2] E.B. Belov, S.V. Lomov, I. Verpoest, T. Peters, D. Roose, RS Parnas, K. Hoes, and H. Sol. Modelling of permeability of textile reinforcements: lattice boltzmann method. *Composites Science and Technology*, 64(7):1069–1080, 2004.

[3] A.L. Berdichevsky and Z. Cai. Preform permeability predictions by self-consistent method and finite element simulation. *Polymer Composites*, 14(2):132–143, 1993.

[4] BR Gebart. Permeability of unidirectional reinforcements for rtm. *Journal of Composite Materials*, 26(8):1100–1133, 1992.

[5] M. Griebel and M. Klitz. Homogenization and numerical simulation of flow in geometries with textile microstructures. *Multiscale Modeling & Simulation*, 8(4):1439–1460, 2010.

[6] B. Laine, G. Hivet, P. Boisse, F. Boust, SL Lomov, and P. Badel. Permeability of the woven fabric. In *Proc. FPCM-8, 8th International Conference on Flow Processes in Composite Materials*, 2006.

[7] F.R. Phelan Jr and G. Wise. Analysis of transverse flow in aligned fibrous porous media. *Composites Part A: Applied Science and Manufacturing*, 27(1):25–34, 1996.

[8] C. Reichman. *Knitted fabric primer*. National Knitted Outwear Association, 1967.

[9] D. Sage. Mij: A java package for bi-directional communication and data exchange from matlab to imagej/fiji. http://bigwww.epfl.ch/sage/soft/mij/. 2011.

[10] Caroline A Schneider, Wayne S Rasband, and Kevin W Eliceiri. Nih image to imagej: 25 years of image analysis. *Nature Methods*, 9(7):671–675, 2012.

[11] D.J. Spencer. *Knitting Technology (third edition)*. Woodhead Publishing, 2001.

[12] B. Verleye, R. Croce, M. Griebel, M. Klitz, S.V. Lomov, G. Morren, H. Sol, I. Verpoest, and D. Roose. Permeability of textile reinforcements: Simulation, influence of shear and validation. *Composites Science and Technology*, 68(13):2804–2810, 2008.

[13] B. Verleye, M. Klitz, R. Croce, M. Griebel, S. Lomov, D. Roose, and I. Verpoest. Predicting the permeability of textile reinforcements via a hybrid navierstokes/brinkman solver. In *8th International conference on flow processes in composite materials*, 2006.

[14] B. Verleye, M. Klitz, R. Croce, D. Roose, S. Lomov, and I. Verpoest. *Computation of the Permeability of Textiles*. SFB 611, 2006.

[15] B. Verleye, S.V. Lomov, A. Long, D. Roose, and CC Wong. Permeability of textile reinforcements: efficient prediction and validation. In *Book of abstracts of the papers presented at the Sixteenth International Conference on Composite Materials, July 8-13, 2007: Kyoto Japan*, pages 220–221, 2007.

[16] I. Verpoest and S.V. Lomov. Virtual textile composites software wisetex: Integration with micro-mechanical, permeability and structural analysis. *Composites Science and Technology*, 65(15):2563–2574, 2005.

[17] CC Wong, AC Long, M. Sherburn, F. Robitaille, P. Harrison, and CD Rudd. Comparisons of novel and efficient approaches for permeability prediction based on the fabric architecture. *Composites Part A: Applied Science and Manufacturing*, 37(6):847–857, 2006.

MOX Technical Reports, last issues

Dipartimento di Matematica "F. Brioschi",
Politecnico di Milano, Via Bonardi 9 - 20133 Milano (Italy)

32/2013 Taddei, T.; Perotto, S.; Quarteroni, A.
Reduced basis techniques for nonlinear conservation laws

31/2013 Dassi, F.; Ettinger, B.; Perotto, S.; Sangalli, L.M.
A mesh simplification strategy for a spatial regression analysis over the cortical surface of the brain

30/2013 Cagnoni, D.; Agostini, F.; Christen, T.; de Falco, C.; Parolini, N.; Stevanović, I.
Multiphysics simulation of corona discharge induced ionic wind

29/2013 Lassila, T.; Manzoni, A.; Quarteroni, A.; Rozza, G.
Model order reduction in fluid dynamics: challenges and perspectives

28/2013 Ekin, T.; Ieva, F.; Ruggeri, F.; Soyer, R.
Statistical Issues in Medical Fraud Assessment

27/2013 Tagliabue, A.; Dede', L.; Quarteroni, A.
Isogeometric Analysis and Error Estimates for High Order Partial Differential Equations in Fluid Dynamics

24/2013 Mazzieri, I.; Stupazzini, M.; Guidotti, R.; Smerzini, C.
SPEED-SPectral Elements in Elastodynamics with Discontinuous Galerkin: a non-conforming approach for 3D multi-scale problems

25/2013 Cattaneo, Laura; Zunino, Paolo
Computational models for coupling tissue perfusion and microcirculation

26/2013 Ieva, F.; Paganoni, A.M.
Detecting and visualizing outliers in provider profiling via funnel plots and mixed effect models

23/2013 Srensen, H.; Goldsmith, J.; Sangalli, L.M.
An introduction with medical applications to functional data analysis